UNIVERSITY OF HELSINKI REPORT SERIES IN PHYSICS

HU-P-D110

APPLICATIONS OF THEORY AND EXPERIMENTS TO ELASTIC SCATTERING IN ION BEAM ANALYSIS

Petteri Pusa

Accelerator Laboratory
Department of Physical Sciences
Faculty of Science
University of Helsinki
Helsinki, Finland

ACADEMIC DISSERTATION

To be presented, with the permission of the Faculty of Science of the University of Helsinki, for public criticism in the Small Auditorium E204 of the Department of Physical Sciences, on February 7th, 2004, at twelve noon.

HELSINKI 2004

ISBN 952-10-0945-4
ISSN 0356-0961
Helsinki 2004
Yliopistopaino

ISBN 952-10-0946-2 (PDF version)
http://ethesis.helsinki.fi/
Helsinki 2004
Helsingin yliopiston verkkojulkaisut

P. Pusa: **APPLICATIONS OF THEORY AND EXPERIMENTS TO ELASTIC SCATTERING IN ION BEAM ANALYSIS**, University of Helsinki, 2004, 30 p.+appendices, University of Helsinki Report Series in Physics, HU-P-D110, ISSN 0356-0961, ISBN 952-10-0945-4 (printed version), ISBN 952-10-0946-2 (PDF version)

Classification (INSPEC): A2410
Keywords: Elastic scattering cross sections, ion beam analysis, Monte Carlo simulations

ABSTRACT

The application of theory and experiments to the elastic scattering in ion beam techniques has been investigated. Experimental elastic scattering cross sections for α + Ni, p + α, ^{7}Li + Ni, ^{11}B + Ni and C + ^{127}I scattering systems have been determined. The optical model and R-matrix analyses have been applied to the experimental data. The calculated cross sections were found to be in very good agreement with the experimental data. The use of the elastic scattering cross sections in ion beam analysis is reviewed from the viewpoint of the calculated data. A computer code for elastic backscattering simulations by using an ion packet Monte Carlo method is introduced.

CONTENTS

1 INTRODUCTION

Particle accelerators have originally been designed to be the main experimental tool in nuclear physics. The development of accelerators has gone through early Cockroft-Walton accelerators up to synchrotron and linear accelerators used in modern high energy particle physics. The particle energies obtained from these accelerators have grown from a few hundred keV's producing the first light element nuclear reactions up to TeV -energies needed in search for the sub-nucleonic constituents.

The rapid development of microelectronics, started in the 1970s, has created the need for characterization and modification of materials having very thin structures, up to this day the sizes of the structures have diminished down to nm range. Ion beam techniques have proven to be the most powerful tools for sub-surface characterization of these materials. Strong development of these techniques undergoes as a response to the increasing challenges of materials science. Energies used in modern ion beam analysis techniques range from a few keV's to several hundred MeV's. The well established accelerator technology and accelerators originally designed for the use of nuclear physics, as well as the achievements in nuclear physics make a strong basis for ion beam analysis. Modern ion beam analysis has found its applications in a variety of different fields: e.g., in microelectronics, metallurgy, biology, medicine, geology, archeology and even fine arts.

The advantage of the use of ion beams is due to their ability to penetrate inside a sample where the knowledge of the interactions between the accelerated ion and target material is used in the analysis. The most common ion beam techniques include the elastic ion scattering techniques: Rutherford backscattering spectrometry (RBS) and elastic recoil detection analysis (ERDA). Other widely used techniques are particle induced X- and gamma ray emission analysis (PIXE and PIGE) and nuclear reaction analysis (NRA).

The two first mentioned methods, RBS and ERDA, are the most widely used ion beam analysis methods and the reasons for this are clear: the experimental set up is easy, the running time for a typical experiment is relatively short, the analysis of the results is straightforward although it might

be laborous in some cases, but above all, the information about the depth distributions and elemental compositions in the sample are simultaneously obtained in a single measurement.

The analysis of the scattering technique experiments is essentially based on the knowledge of the scattering probabilities and deceleration of ions in solids, described by differential scattering cross sections and stopping cross sections, respectively. Conventionally a pure elastic point-like Coulomb interaction between the projectile and target nuclei is assumed, and the differential scattering cross section is given by the famous Rutherford formula [1]. The validity of this assumption sets limits to acceptable projectile energies, dependent on the atomic numbers and the masses of the interacting projectile and target pair. At lower energies the effect of the electrons surrounding the nucleus cannot be neglected and the electronic screening begins to diminish the Rutherford scattering cross section smoothly as a function of the projectile energy. At higher energies the projectile eventually approaches the Coulomb barrier of the colliding nuclei. Nuclear interactions begin to occur and they can cause dramatic changes in the scattering cross sections.

The non-Rutherford nuclear interactions complicate especially the analysis of lighter target materials or deep probing analysis where higher energies must be used. On the other hand, the non-Rutherford processes can be used to enhance the detection sensitivity of light elements. Expanding the scattering techniques outside of the pure Rutherford scattering energies also makes these techniques much more versatile but the non-Rutherford scattering cross sections must be known. Since the nuclear models extrapolate cross sections to energies and angles where experimental data do not exist, free choice is achieved in setting up the experimental conditions. A fair amount of literature data for proton or helium as projectile is available but unfortunately only for restricted angles and energies. The data sets also may contain systematic differences compared to each other. The use of nuclear physics theories for modeling the cross sections helps finding and correcting discrepancies in the experimental data.

Most of the frequently used computer programs for scattering spectrum simulations, such as GISA [2], SIMNRA [3], RUMP [4] or IBA DataFurnace [5] can handle non-Rutherford cross sections if the data points have been tabulated into program files. Steps have recently been taken to maintain and develop data banks and calculation tools based on the modeled cross section data [6]. Maintaining

such data bases by an organization like IAEA has many advantages compared to the present situation where the calculated cross sections are available only by individual researchers: the data will be easily available, more reliable and more often updated.

Adding the calculation modules into simulation programs will make the utilization of these programs much more useful and multipurpose. Using this approach of calculating cross sections from the parameters of nuclear models instead of using discrete parameter sets will render possible the simulations of RBS or ERDA spectra at any angle. This possibility is very useful in design and analysis of the scattering experiments.

Limiting factors in the scattering experiments are the multiple scattering effects. The contribution of these varies but can be crucial in many cases. In order to simulate these effects the scattering cross sections must be known at all scattering angles and at energies below the initial projectile energy. In practice the only possible source for the non-Rutherford cross sections in this case are the modeled cross sections.

2 PURPOSE AND STRUCTURE OF THIS STUDY

The purpose of the present study is to extend the usability of the most important ion beam techniques of materials science, RBS and ERDA, to cases where projectile energies fall outside the window of Rutherford elastic scattering. This includes the application of nuclear physics theories, presentation of new elastic cross section data and development of the scattering computer simulations. The experimental cross section data are fitted by using optical model and R-matrix theories. The calculated cross sections are less affected by the statistical and sometimes systematical errors than the experimental data. Furthermore, the models enable computer simulations where multiple scattering effects are involved. The application of theory and experiments to the ion beam analysis will be investigated.

In articles I and II new experimental cross sections are measurements are described and analyzed by nuclear models mainly for the use of backscattering spectrometry. In articles III and IV new cross section data are presented and a similar theoretical treatment is carried out for applications in ERDA. The Monte Carlo calculations for ion backscattering are investigated and an ion packet –method for fast non-Rutherford backscattering simulations is introduced in article V.

After the introduction and Section 2 of the thesis the experimental work, models and the used fitting procedures are described in Section 3. In Section 4 the existing cross section literature data suitable for the needs of ion beam analysis are briefly reviewed with examples from the articles of this work and from the literature. The use of computer simulations is also discussed in this section. Conclusions with ideas for the future research in this field are given in the last Section 5.

Summaries of the original articles

Article I: ^{4}He + Ni elastic scattering near the Coulomb barrier and optical model parameters, A. Nurmela, P. Pusa, E. Rauhala and J. Räisänen, *Journal of Applied Physics* **91** (2002) 2438.

Elastic scattering cross sections were measured for ^{4}He scattering by nickel. An optical model parameterization was given for the cross section data. Rutherford scattering threshold limits and non-

Rutherford cross sections are presented for the ^{4}He + Ni scattering system at all scattering angles and measured energies by using the optical model.

Article II: RBS and ERD cross sections and optical model parameters for the analysis of lithium, boron and nickel, A. Nurmela, P. Pusa, E. Rauhala and J. Räisänen, *Nuclear Instruments and Methods in Physics Research B* **161-163** (2000) 130.

Rutherford scattering threshold limits and new elastic scattering cross sections were determined for Ni by using ^{7}Li and ^{11}B as projectiles. Optical model parameters were fitted to the experimental cross sections.

Article III: Elastic scattering in the iodine-carbon system near the Coulomb barrier, P. Pusa, E. Rauhala, T. Alanko and J. Räisänen, *Journal of Applied Physics* **93** (2003) 6370.

The studies of the cross sections for light ions in articles I and II are further extended to heavier ions. High energy heavy ion ERDA scattering cross sections were determined by using the inverse C(^{127}I,C)^{127}I scattering process. The obtained cross sections were analyzed with the optical model. The calculated cross sections are given for all scattering angles and energies used.

Article IV: Alpha - proton elastic scattering cross sections for ERDA in the resonance region, P. Pusa, E. Rauhala, A. Gurbich and A. Nurmela, *Submitted to Nuclear Instruments and Methods in Physics Research B.*

Elastic scattering cross sections were measured for the p - α system in the strong resonance region. The obtained cross sections together with available literature data in the resonance region were modeled by using the R-matrix theory. The results obtained suggest changes to the previous R-matrix parameterization in the resonance region.

Article V: Fast Monte Carlo simulation for elastic ion backscattering, P. Pusa, T. Ahlgren and E. Rauhala, *Accepted for publication in Nuclear Instruments and Methods in Physics Research B.*

A fast Monte Carlo simulation procedure using ion packet method for ion elastic backscattering is presented in this article. The non-Rutherford scattering cross sections are easily imple-

mented in this model. The methods of utilizing the nuclear models developed in articles I–IV were applied in this article for the calculation of the multiple scattering contribution.

The articles presented in this thesis are the result of group work. My contribution in articles I-IV was the evaluation of the obtained cross sections by the optical model and R-matrix theory. I was responsible for the experimental work and data analysis in articles III and IV and participated in the measurements in articles I and II. In article V, I was responsible for the development of the ion packet method and the design of the computer program. I was the corresponding author in articles III-V.

3 ELASTIC SCATTERING IN ION BEAM ANALYSIS

In general, the interaction of energetic ions in the target material consists of elastic and inelastic collisions between nuclei and electrons. In the case of an elastic scattering process the momentum and kinetic energy between the colliding nuclei, projectile and target, are conserved. The relevant quantities to be considered are the elastic kinematical factors and the elastic scattering cross sections. The stopping cross section describes the deceleration of the projectile in the target material and results from electronic stopping and nuclear stopping parts. The electronic stopping describes the complex electron-electron and electron-nucleus interactions, while the nuclear part of the stopping consists of the energy lost due to momentum transfers in the nuclear binary collisions.

In the laboratory frame of reference the elastic collision can be seen either as a scattering or a recoil process. In the scattering process the incoming projectile is of primary interest after the collision, whereas in the recoil process the recoiled target nucleus is followed and detected, see Fig. 1. The techniques of ion beam analysis, RBS and ERDA are based on these scattering processes. Detailed descriptions of the techniques are found, e.g., in Ref. [7]. The time-of-flight technique used to detect the recoiled target atoms in ERDA, see Fig. 1, is extensively studied in Ref. [8].

The differential scattering cross section in the pure Coulomb field, the Rutherford cross section, is given in the center of mass frame by

$$\frac{d\sigma}{d\Omega} = \left(\frac{Z_1 Z_2 e^2}{4E} \right)^2 \frac{1}{\sin^4 \frac{\theta}{2}}, \tag{1}$$

where E is the center of mass energy, e^2 the constant 1.44 MeVfm, Z_1 and Z_2 are the projectile and target nucleus atomic numbers, respectively, and θ is the center of mass scattering angle. It is noteworthy that the same result for the Rutherford scattering cross section is obtained by both the classical and the quantum mechanical treatment.

The utilization of the stopping cross sections, elastic kinematics and scattering cross sections, either Rutherford or non-Rutherford, prepares the way for the elastic scattering spectrum analysis for

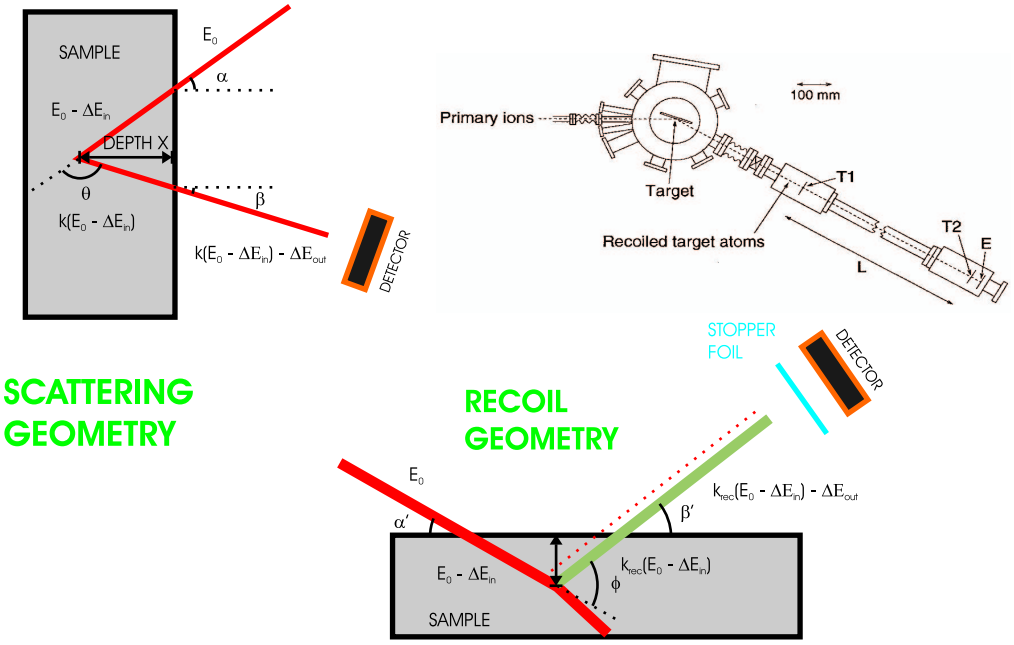

Figure 1: Scattering and recoil geometries. The corresponding scattering and recoil angles are denoted by θ and ϕ, entrance and exit angles by α/β and α'/β' , the kinematical factors by k and k_{rec}, the initial energies by E_0 and the energy losses by ΔE. In the recoil geometry the unwanted scattered ions or recoils are often filtered by a stopping foil in front of the detector. The figure at top right shows the time-of-flight ERDA setup at the University of Helsinki, the energy detector is used to separate different masses in coincidence with the time-of-flight signal.

elemental isotopic depth profiling.

3.1 Experimental procedures

The scattering cross section data presented in the articles of this study have been determined by using three different experimental techniques.

i) In articles I and II an internal Rutherford dose reference was employed. The sample was composed of thin layers of gold and nickel, nickel being the studied element and gold the internal dose reference. The scattered yield recorded in a detector caused by an ion beam traveling through an elemental foil can be expressed as:

$$Y = Q \int_{E_1}^{E_0} dE \frac{1}{S(E)} \frac{d\sigma(E)}{d\Omega} \Delta\Omega, \tag{2}$$

where Q is the number of projectiles entered into the foil (fluence), E_0 and E_1 are the beam energies before and after the foil, $S(E)$ is the stopping cross section, $\frac{d\sigma(E)}{d\Omega}$ is the differential scattering cross section and $\Delta\Omega$ the solid angle of the detector, here assumed to be point-like. For thin layers the formula can be approximated as

$$Y = QN_t \frac{d\sigma(\bar{E})}{d\Omega}\Delta\Omega, \tag{3}$$

where N_t is the areal density of the layer and $\bar{E}$ the mean energy of the beam in the layer. This approximation is valid if the scattering cross section changes linearly in the interval $E_0...E_1$. The conditions above were fulfilled in the experiments of the present work. Eq. (3) was first used to obtain the N_t ratios for gold and nickel at beam energies where the scattering was known to be Rutherford. The same equation was then used to determine the non-Rutherford cross sections by collecting the yields from the Ni and the Au layers.

ii) In article IV the cross sections were determined in a similar manner by measuring the yield ratios for the Rutherford reference and He yields and applying Eq. (3) to find the cross sections. It wasn't possible to obtain the areal density for the implanted ^{4}He by backscattering because scattering cross sections of any lighter element for ^{4}He are not Rutherford at sufficient energies to determine the reference and the ^{4}He N_t ratios simultaneously. The ^{4}He areal density was found by simultaneous recoil transmission and backscattering measurement of a 20 MeV ^{28}Si beam. The recoiled ^{4}He atoms were filtered by a stopper foil into the recoil detector. The Ta reference front edge height H of the backscattered ^{28}Si was used to determine the beam fluence by

$$H = \frac{Q\delta E}{[\epsilon_0]\cos\alpha}\frac{d\sigma(E_0)}{d\Omega}\Delta\Omega, \tag{4}$$

where δE is the energy - channel calibration, $[\epsilon_0]$ is the stopping cross section factor and α the angle between the incoming beam and the sample normal. The obtained fluence was substituted into Eq. (3) for the determination of the ^{4}He areal density.

ii) In article III the cross sections were also obtained by applying Eq. (3) in the recoil transmission geometry. A Faraday cup was set behind the sample and it collected the beam charge for each set of

angular distribution measurements. The integrated charge, proportional to Q, was used to normalize the different data sets. The obtained cross sections were further normalized to Rutherford at known angles, which also determined the remaining constant factors $\Delta\Omega$, N_t and factors affecting the charge collection: recoiled carbon, secondary electrons and different projectile charge states.

The use of an internal dose reference, as in cases i) & ii), is the most accurate of these methods. The error source is essentially related to the statistics gained, the accuracy can always be enhanced by increasing the measurement time. In ii) an additional error source arises from the ^{4}He areal density determination. This was due to uncertainties in the measurement of the solid angles for detectors and from the uncertainty in the stopping cross section factor in Eq. (4). Since tantalum stopping for ^{4}He was believed to be more accurate than for ^{28}Si, a tantalum layer was evaporated on a Si substrate and backscattering spectra were taken with ^{4}He and ^{28}Si beams. From these measurements a correction of a factor of 1.03 was obtained for the stopping cross section of Ta for ^{28}Si. In the case iii) additional errors arose from the difficulty of the exact determination of the scattering angles.

3.2 Optical model theory

The elastic cross sections for potential scattering in the articles I–III have been calculated by using the optical model potential

$$V(r) = V_C(r) + V_n(r) + iW_n(r), \tag{5}$$

where $V_n(r)$ is the real part of the nuclear potential and $W_n(r)$ the imaginary part. The term $V_C(r)$, the Coulomb potential of a uniformly charged sphere, is defined as:

$$\begin{aligned} V_C(r) &= \frac{e^2}{r}\left[\frac{3r}{2R_C} - \frac{1}{2}(\frac{r}{R_C})^3\right], r \leq R_C \\ V_C(r) &= \frac{e^2}{r} \qquad\qquad\qquad\qquad , r > R_C, \end{aligned} \tag{6}$$

with the Coulomb radius R_C. The most popular form of both real and imaginary parts of the nuclear potential found in the literature is the Saxon-Woods form factor

$$f(r,R,a) = \left(1 + \exp(\frac{r-R}{a})\right)^{-1}, \tag{7}$$

which is characterized by the nuclear radius R and the surface diffuseness a, these geometry parameters are often different for real and imaginary parts of the nuclear potential. The Saxon-Woods nuclear potential forms and its derivatives are also used in the articles presented in this study.

The radial Schrödinger equation is solved for each partial wave by following the procedure described, e.g, in [9]. As the nuclear matrix elements S_l are solved, the elastic differential scattering cross section with respect to Rutherford can be expressed as:

$$\frac{d\sigma}{d\sigma_{Ruth}} = |-e^{2i\sigma_0 - 2i\eta \ln \sin\frac{\theta}{2}} + \frac{\sin^2\frac{\theta}{2}}{i\eta}\sum_{l=0}^{\infty}(2l+1)(S_l-1)e^{2i\sigma_l}P_l(\cos\theta)|^2, \tag{8}$$

where η is the Sommerfeld parameter, θ the center of mass scattering angle, σ_l the Coulomb phase shift and P_l the Legendre polynomial of l^{th} degree. Breit-Wigner resonances can be added to the S-matrix, an often applied convention is presented e.g. in [10].

3.3 R-matrix theory

The elastic scattering cross sections in article IV are calculated by using the R-matrix theory, the calculation procedure used in the article IV is given below. In the R-matrix theory the compound nucleus states are labeled in terms of the reduced energy widths and eigenenergies. A complete description of this theory is given in Ref. [11]. The R-matrix is defined as

$$R_l^{\pm}(E) = \sum_{\lambda}\frac{\gamma_\lambda^2}{E_\lambda - E}, \tag{9}$$

where γ_λ are the reduced level energy widths and E_λ the level eigenenergies. Indice l corresponds to the orbital angular momentum quantum number and $\pm$ to the spin state, e.g. R_1^+ is the R-matrix

element for the $p_{3/2}$ state. The nuclear phase shifts are given by

$$\delta_l^{\pm} = \arctan \frac{R_l^{\pm} P_l}{1 - R_l^{\pm} S_l} + \phi_l, \tag{10}$$

where

$$S_l = \frac{\rho(F_l F_l' + G_l G_l')}{F_l^2 + G_l^2}, \qquad \rho = ka \tag{11}$$

and

$$P_l = \frac{\rho}{F_l^2 + G_l^2}, \tag{12}$$

where k is the wave number of the relative motion and a is defined as the interaction radius. The regular and irregular Coulomb functions are denoted as F_l and G_l, respectively. A fast numerical procedure for calculating the Coulomb functions at all energies and ρ is given in Ref. [12]. The variable ϕ_l is defined as the hard sphere phase shift and is given by

$$\phi_l = -\arctan \frac{F_l}{G_l}. \tag{13}$$

The differential cross section is expressed in terms of the scattering amplitudes A and B as

$$\frac{d\sigma}{d\Omega} = |A|^2 + |B^2|. \tag{14}$$

The amplitudes are calculated from the relations

$$A = f_C + \frac{1}{2ik} \sum_{l=0}^{\infty} \left((l+1) S_l^+ + l S_l^- - (2l+1) \right) e^{2i\sigma_l} P_l(\cos\theta) \tag{15}$$

and

$$B = \frac{1}{2ik} \sum_{l=1}^{\infty} \left(S_l^+ - S_l^- \right) e^{2i\sigma_l} P_l^1(\cos\theta), \tag{16}$$

where P_l^1 is an associated Legendre polynomial and $S_l^{\pm} = e^{2i\delta_l^{\pm}}$. The Coulomb amplitude f_C is given by

$$f_C = -\frac{n}{2k \sin^2 \theta/2} e^{-i\eta \ln(\sin^2 \theta/2) + 2i\sigma_0}. \tag{17}$$

3.4 Screening

Several alternative representations for describing the electronic screening have been given in the literature. In the case of weak screening, a relatively simple analytic formula has been shown to be in good agreement with experimental data [13]:

$$\frac{d\sigma}{d\sigma_R} = \frac{(1 + V_1/(2E))^2}{(1 + V_1/E + V_1/(2E)(1/\sin\frac{\theta}{2}))^2}, \tag{18}$$

where $V_1 = 0.04873 Z_1 Z_2 (Z_1^{2/3} + Z_2^{2/3})^{1/2}$, the energy E is given in keV and θ is the center of mass scattering angle. Cross sections reproduced by Eq. (18) have been also compared with those obtained by Monte Carlo calculation program TRIM [14] and were found to be in good agreement even for energies as low as 200 keV. The screening correction has been negligible in all the non-Rutherford measurements in articles I–IV and has not been taken into account. However, in the case of low energy and small angle scattering in Monte Carlo simulations it has to be included in the calculations in order to produce realistic spectra, see article V.

3.5 Fitting procedure

The χ^2 test has been used as a statistical goodness of the fit indicator for the the optical model and R-matrix parameters throughout all the articles of this study. It is defined (per point) as

$$\chi^2 = \frac{1}{N} \sum_{k=1}^{N} \left(\frac{\sigma_k^T - \sigma_k^E}{\delta\sigma_k^E} \right)^2, \tag{19}$$

where N is the number of data points, σ is the cross section value (or other observable) and $\delta\sigma$ the uncertainty of σ. Superscripts T and E refer to the theoretical and experimental values, respectively. Several different fitting methods are presented in the literature. These can roughly be divided into two categories: the systematic variation of the fitting parameters or the use of the χ^2 gradient to give the direction of steepest descent in the parameter space. A pitfall of the optimization procedure is to end up in a ”wrong”, local minimum of the χ^2 function. The applied approach has been the following:

1) Map the physically sensible limits for the parameters.

2) Calculate a χ^2 grid as dense as possible in this parameter space.

3) Discard the clearly incorrect subspace.

4) Use the remaining space as the initial values for different kind of search routines.

The initial value is often crucial for a successful fit. Therefore the obtained result is the more reliable the more different initial parameter sets end up in the same solution. In the case of the optical model additional ambiguities follow, such as Igo or discrete ambiguities, see, e.g., [15]. These can be taken into account in the search routines by knowing the systematics of the Igo ambiguity and by fitting several energies simultaneously and demanding the same geometrical parameters for the optical potentials. The fitting procedure outlined above has been applied in articles I–IV.

4 CALCULATED DATA AND COMPUTER SIMULATIONS

4.1 Existing data

A large amount of scattering data can be found in the literature. An INSPEC database search with keywords ”elastic scattering” + ”nucleus” gives over 6500 hits. However, the majority of these data are related to nuclear physics research and unfortunately - from the point of view of the present needs - the studied scattering systems and energies do not have much use in ion beam analysis. Most of the published experimental cross section data applicable to the ion beam analysis have been collected into the SIGMABASE website [16].

At present there are no general databases available for calculated cross section data. By calculated data we denote cross sections fitted to the experimental data by nuclear models. The term evaluation is sometimes also used to mean the critical assessment of experimental cross section data by nuclear model fitting. Recently a cross section calculation tool for RBS has been under development, which can be used to obtain some elastic proton and α-particle resonance reaction cross sections [17]. The existing literature data for the calculated cross sections that are considered significant in the applications of ion beam analysis are listed in Table 1.

Calculated proton cross sections can be found in the literature for carbon, oxygen, nitrogen, aluminum and silicon, all very common elements analyzed in backscattering spectrometry. The ^{4}He(p,p) cross sections are especially useful in the reverse ERDA process of detecting hydrogen due a strong elastic resonance. The overall fits for heavier targets are mainly useful in deep probing measurements and for finding the Rutherford threshold limits. Important calculated cross sections missing for the light elements are for p + d and p + F systems.

In the case of the α-particle the calculated data are few. Only the calculated behavior of C + α, ^{16}O + α and Ni + α is known in the Rutherford energy region and above.

Proton and α-particle beams are the most widely used probing beams for RBS. Being light particles

their Rutherford thresholds with lighter target materials appear at relatively low energies. It is thus important to know these limits accurately. On the other hand the collisions of light elements often lead to compound nucleus scattering. This may occur as a strong resonance structure in the elastic scattering cross section excitation curve. These resonance cross sections may be several hundreds of times stronger than the Rutherford scattering cross sections. If the cross sections are known and can be modeled, the use of non-Rutherford cross sections provides a great advantage in these cases due to strongly enhanced detection sensitivities. This gives a strong motivation for calculating the experimental data by nuclear models.

Advantages have been pointed out recently for the use of heavier beams, especially lithium [18], in backscattering spectrometry due to their better mass and depth resolution. The calculated cross sections for lithium are known only for carbon and nickel. The I + C scattering cross sections have also been modeled for both heavy ion RBS and heavy ion ERDA, and these results are presented in article III.

The resonant behavior of some elastic scattering cross sections is illustrated in Fig. 2. The enhanced detection sensitivity due to the elastic resonances is widely utilized in backscattering spectrometry for concentration determination or depth profiling. Utilizations of the cross sections of Fig. 2 are found in article V and, e.g., in Refs. [35] and [36]. Strong and narrow resonances are also used for energy calibration of the analyzing magnets, see e.g., [37]. From the experimental point of view the calculated cross sections provide more freedom for selecting the ion energies and scattering angles. If the sample contains more than one element for which the scattering is non-Rutherford the experimental data usually do not cover the same energies and angles.

4.2 Data of this study

The typical behavior of the shape elastic scattering can be seen in the cross sections presented in articles I–III. Deviations from the Rutherford cross sections in the elastic cross section excitation

Table 1: Literature data for the calculated elastic cross sections. The cross section data are converted to scattering geometry of the lighter element to enable comparison of data. If the isotope is not given, the fit has been performed to the most abundant isotope which is assumed to govern the scattering. If the lower energy is not given, the fit is assumed to be valid down to Rutherford scattering. The model applied is either the optical model (OM) or the R-matrix (RM) theory.

Reaction	Validity (MeV)	Angles (deg)	Method	Reference	Comments
^{3}He(p,p)	6.8-16.2	11...173	OM	[19]	
^{4}He(p,p)	≤ 17	15...163	RM	[20]	Several literature data sets
^{4}He(p,p)	≤ 5	80...170	RM	Article IV	
C(p,p)	≤ 3.5	55...170	OM	[21]	Several literature data sets
^{14}N(p,p)	3.7-5.67	67.5...157.5	RM	[22]	
O(p,p)	≤ 4	77...170	OM	[23]	Several literature data sets
^{28}Al(p,p)	0.92-1.85	90...160	RM	[24]	
Si(p,p)	≤ 3	73...170	OM	[25]	Several literature data sets
^{32}S(p,p)	≤ 4	64...163	RM	[26]	
$^{A}_{Z}$X(p,p)	9-22	20...170	OM	[27]	Z>13 overall fit
$^{A}_{Z}$X(p,p)	7-50	15-160	OM	[28]	A>40 overall fit
^{12}C(α,α)	2.6-8.2	24...166	RM	[29]	
C(α,α)	≤ 8	31...171	OM	[30]	Several literature data sets
^{13}C(α,α)	2-3.5	43...165	RM	[31]	
^{16}O(α,α)	≤ 9	90...165	RM	[32]	
^{34}S,^{50}Cr,^{62}Ni(α,α)	12.8-20	20-166	OM	[33]	
Ni(α,α)	≤ 14.3	30-165	OM	Article I	
^{12}C(^{6}Li,^{6}Li)					
^{12}C(^{7}Li,^{7}Li)	4.5-13	6...120	OM	[34]	
Ni(^{7}Li,^{7}Li)*					
Ni(^{11}B,^{11}B)	$\leq 15^{*}, \leq 24$	89, 110*, 132*	OM	Article II	
^{127}I(C,C)	$\leq$50	27...137	OM	Article III	

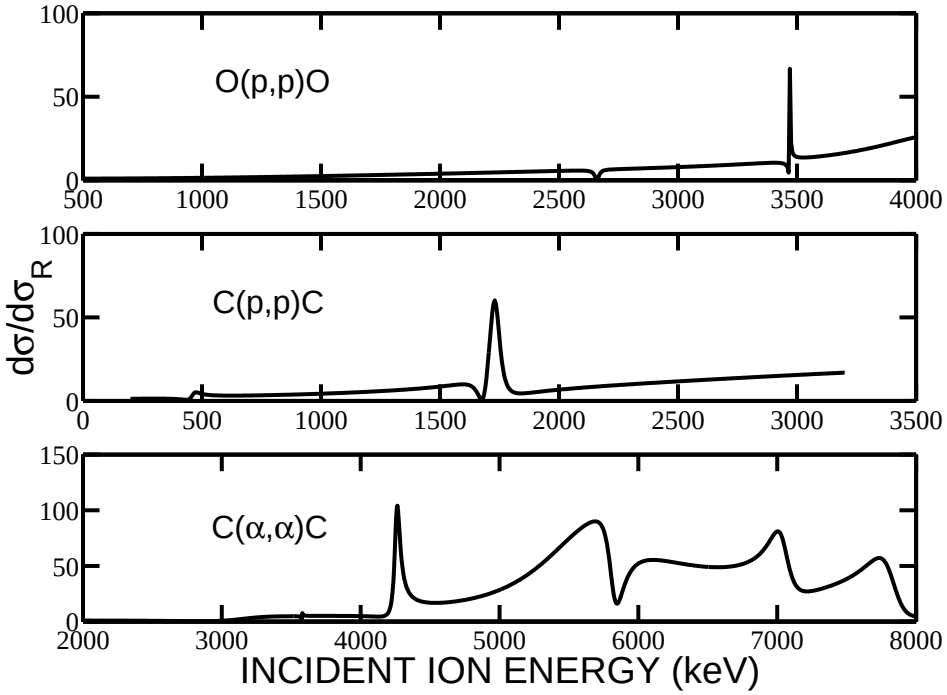

Figure 2: Calculated proton elastic scattering cross sections for oxygen and carbon and α elastic scattering by carbon. The optical model parameters are taken from Refs. [23], [21] and [30], respectively. The calculations were performed for the projectile laboratory backscattering angle of 170°.

curves depart smoothly as a function of energy. In articles I and III the geometrical parameters for the optical model have been fitted to experimental angular distributions. The energy dependencies of the potential well depths have been investigated by keeping the geometrical parameters constant. In article II no angular distributions were available for the fit. Therefore, the extrapolations of the optical model predictions into the whole angular plane are assumed to be more reliable in articles I and III.

In article I the Rutherford threshold limits for the Ni + α system and non-Rutherford scattering scattering cross sections are determined up to the center of mass energy of 13.4 MeV. Deep probing analysis by using either RBS or ERDA for this elemental pair has applications in, e.g., materials research for fusion reactors, semiconductor technology and metallurgy (e.g., Refs. [38] and [39]). Heavy ion high energy ERDA has advantages for probing the sample even up to μm ranges and detecting a wide range of masses simultaneously. These advantages for use of high energy ^{127}I ERDA up to 3.3 MeV/u have been pointed out in Refs. [40], [41] and [42]. The recoil elastic cross sections for ^{127}I + C are drawn in Fig. 3 as a function of C recoil angle and ^{127}I probing energy. The calculations are based on the optical model analysis of article III. It can be seen from Fig. 4 of article III that the scattering deviates

from Rutherford for C(^{127}I,C)^{127}I already below 3.3 MeV/u (419 MeV ^{127}I beam energy). For such high energy analysis the knowledge of the scattering cross sections and the upper energy limit of the Rutherford window are of primary importance. Several analytical or semiempirical models exist for predicting the non-Rutherford threshold energies. All models give reasonable overall behavior for the threshold energy but for individual ion-target pairs the predicted threshold energy may significantly deviate from the experimental threshold [43], [44], [45], [46].

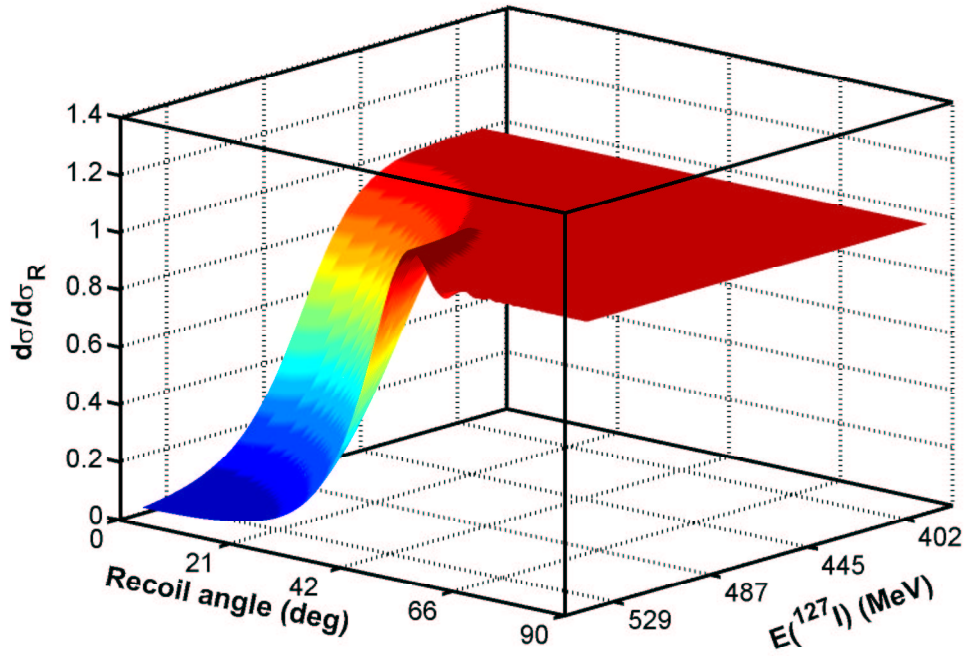

Figure 3: Elastic scattering cross section behavior for C(^{127}I,C)^{127}I plotted as ratio to Rutherford in the energy-angle –plane near the Coulomb barrier.

Hydrogen is one of the most studied elements by ion beam analysis. It is probed either by ERDA or NRA. The surface depth resolution by using He ERDA has been found to be about 60 nm in Al [47]. The p + α scattering system has a broad elastic resonance at a center of mass energy of 1.8 MeV. At the resonance the cross section is enhanced by several hundred fold as compared to the Rutherford cross section. The p-α cross sections have been studied in article IV by using R-matrix analysis. The modeled cross sections are drawn in Fig. 4 together with the experimental data used in the R-matrix fit.

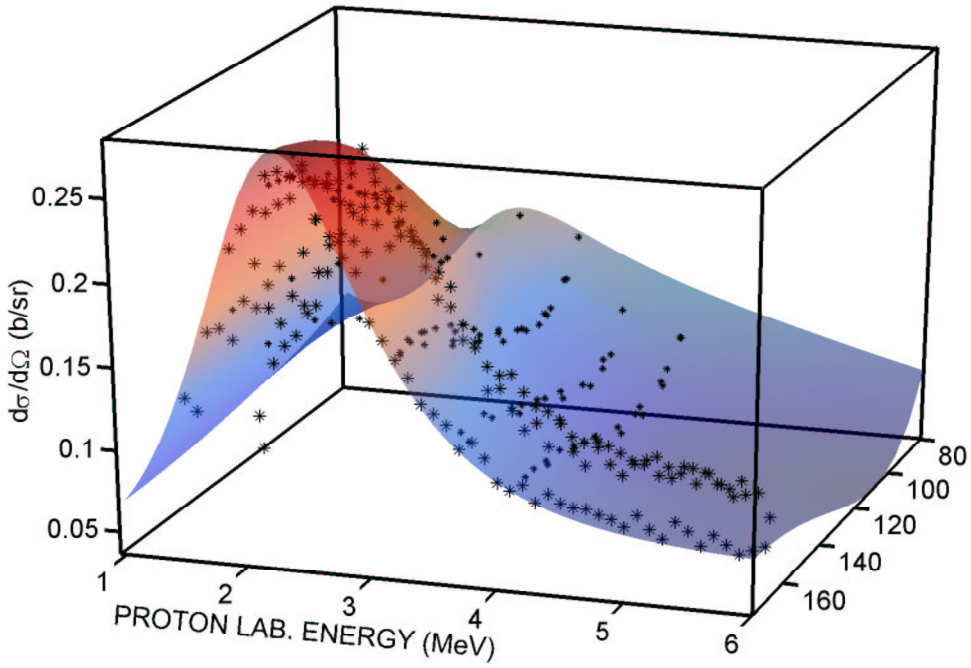

Figure 4: The broad proton-α resonance at p backscattering angles. Available earlier literature data, plotted as *, are shown with the experimental cross sections of article IV. References to literature data are found in article IV. The cross sections are calculated by the R-matrix theory with parameters presented in article IV.

The proton-α cross sections have been modeled earlier in Ref. [20] through an extensive set of experimental data. The present fit was found to deviate from the previous one at the resonance region. This is illustrated in Fig. 5. The fit given in article IV gives almost 15% lower values for large backscattering angles than the fit from Ref. [20]. The difference directly affects the determined hydrogen content in case the calculated cross sections are used in spectrum data analysis. The R-matrix parameterization from article IV is therefore suggested to replace the earlier parameterization when the cross sections for recoil hydrogen detection by ^{4}He are needed.

4.3 Computer simulations

The computer simulations in spectrum data analysis are based on the principles presented in Section 3. The investigated quantities are the elemental distributions, concentrations and the stoichiometry of the sample. Iterative simulation steps are often required for ending up to the final result [48]. The idea

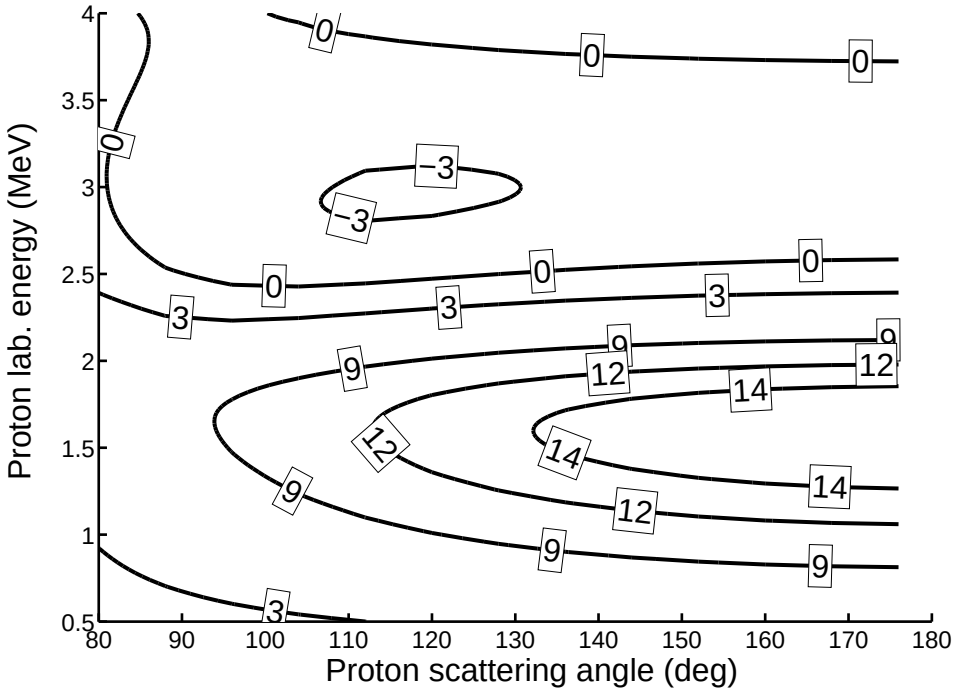

Figure 5: Comparison with previous R-matrix fit [20] and the one presented in article IV at the resonance region. The contour numbers indicate the difference of the two fits in percent. The positive numbers indicate lower values for the fit of article IV.

of the single scattering ('analytical') model is that the sample is divided into thin slabs. The incoming ion beam energies are calculated through the slabs and the scattering yields are obtained. With modern computer capacity such a calculation is very fast and the iteration can be easily performed.

Multiple scattering effects can, however, contribute significantly or even dominantly to the experimental spectra [49]. This is especially the case at small scattering angles and low ion energies or if the ion path in the sample is long (i.e., for deep probing analysis or in low energy tails of the scattering spectra). Adding these contributions to analytical models makes them very slow and not suitable for iterative spectrum fitting. Considerable difficulties are also encountered if non-Rutherford cross sections are used. The multiple scattering is an even more serious problem in ERDA. Also, sample surface roughness complicates the ERDA simulations [50], [51].

Monte Carlo simulations offer the most realistic description of ion scattering. Conventionally simulations are based on following a single ion in the sample. Since especially the backscattering probabilities are very small, the running time for such a simulation is very long. Article V is focused on

this issue. A significantly faster Monte Carlo method for ion backscattering is developed introducing the ion packet method, used for neutron scattering in Ref. [52] and described in detail in article V. The simulation time can be reduced to a few minutes enabling the use of the iterative fitting steps in a reasonable time. The non-Rutherford cross sections are readily included into this model. The strong contributions of the 'unwanted' multiple scattering effects are studied, e.g., in Ref. [53] in the case of deep probing protons in carbon and in the presence of strong elastic resonances. Fig. 6 shows the different multiple scattering contributions to the RBS resonant yield for a non-Rutherford excitation curve.

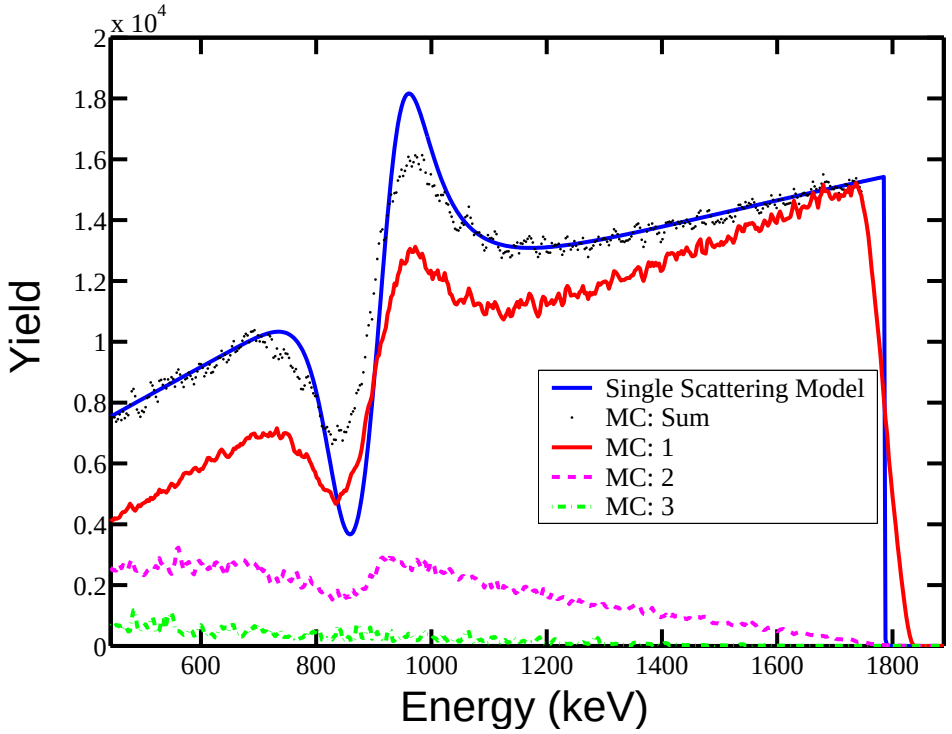

Figure 6: Backscattering of 2.3 MeV protons by carbon at the scattering angle of 110° calculated with the ion packet method. Comparison with the single scattering model. The cross sections are obtained by using the parameters taken from Ref. [21] in the optical model calculation. MC1, MC2 and MC3 refer to 1-, 2-, and 3–fold scattering, MC sum is the sum of these contributions.

Fig. 7 illustrates the broadening of the scattering yield due to the multiple scattering effects in the presence of the sharp resonance of O(p,p)O, see Fig 2. The broadening effect has also been the subject of study in Ref. [53]. If the nuclear excitation function has sharp resonances they must be carefully taken into account in the analysis, see Ref. [54].

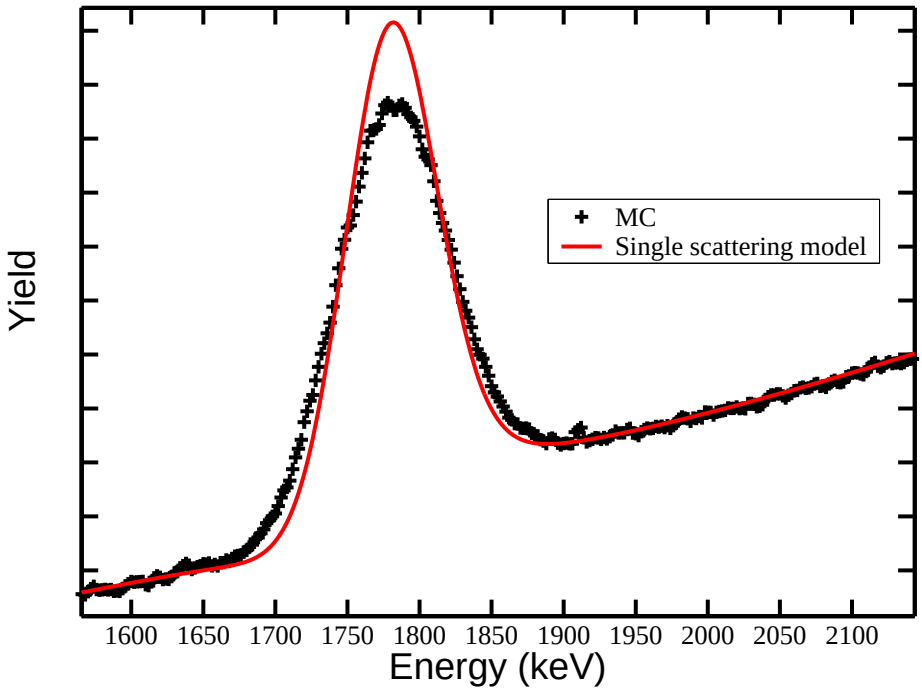

Figure 7: Proton elastic backscattering yield by oxygen calculated both by the packet Monte Carlo method and the single scattering model. The cross sections are calculated by using the parameters of Ref. [23].

5 CONCLUSIONS

The application of theory and experiments to the elastic scattering in ion beam techniques has been investigated. In the articles presented in this thesis the elastic scattering cross sections have been measured for the following scattering systems; α + Ni, p + α, ^{7}Li + Ni, ^{11}B + Ni and C + ^{127}I. The measured cross sections have been modeled by either optical model or R-matrix analysis. The applied models were found to reproduce the experimentally determined cross sections with very good agreement. The models have enabled the investigation of the cross sections in the entire energy-angle –plane below the measured energies. The obtained results can be used as a source for cross sections when beam energies beyond the Rutherford threshold limits are used and for determination of the threshold energies. In article V the principle for a fast Monte Carlo code is presented. The code developed enables the simulation of non-Rutherford backscattering spectra with multiple scattering effects included in a reasonable time.

As indicated in Section 4.1, the calculated parameters for cross section determination of proton elastic

scattering are often available, but not for heavier projectiles. Especially ^{4}He and ^{7}Li elastic scattering cross sections for various target elements are frequently needed by the ion beam analysis community but the calculated cross sections are only available in rare cases. The calculation of these cross sections would thus be important for the community. In many cases additional experimentally determined cross section values are required besides the data now available in the literature.

The analysis of RBS and ERDA spectra in the general case calls for elastic scattering cross sections for all angles and wide ranges of energies. The methods and techniques developed in this thesis make the spectrum analysis feasible when experimental scattering cross sections are not available for the desired angles or in the presence of sharp resonances and multiple scattering. With the increasing computer capacity, procedures using nuclear models and fast Monte Carlo calculations can be incorporated directly into the data analysis software to facilitate spectrum data analysis even in these complicated cases.

In the near future we will investigate the p + d elastic cross sections and carry out the calculation procedure. The d(p,p)d cross section is several hundred fold larger compared to Rutherford cross section making the determination of deuterium concentration by protons feasible. The Monte Carlo code presented in article V is presently capable of handling only one target layer. It will be further developed to include the possibility for multilayer analysis.

ACKNOWLEDGEMENTS

I am deeply indebted to Doc. Eero Rauhala for his guidance with this thesis. He has also advised and encouraged me in many areas of my work. I am also grateful to Prof. Jyrki Räisänen for many enlightening discussions.

I wish to thank Prof. Juhani Keinonen for providing me the possibility to work at the Accelerator laboratory.

I wish to thank all my colleagues for their comments and criticism, especially Prof. Tommy Ahlgren, Dr. Timo Sajavaara, Dr. Kai Arstila, Dr. Arto Nurmela and MSc Kalle Heinola. The atmosphere in the Accelerator Laboratory has made working there most enjoyable.

Finally, I wish to thank Sirke Happonen for all her support and patience.

Financial support from the Magnus Ehrnrooth foundation, the Academy of Finland and the Univ. of Helsinki Chancellor's travel fund is gratefully acknowledged.

Helsinki, January 2004

Petteri Pusa

REFERENCES

1. E. Rutherford, Phil. Mag. **21** (1911) 669.
2. GISA computer program, J. Saarilahti and E. Rauhala, Nucl. Instr. and Meth. B **64** (1992) 734.
3. SIMNRA computer program, http://www.rzg.mpg.de/ mam/.
4. RUMP computer program, L. Doolittle, NIM **B 9** (1985) 291.
5. C. Jeynes, N. P. Barradas, P. K. Marriott, G. Boudreaud, M. Jenkin, E. Wendler and R. P. Webb, J. Phys D: Appl. Phys. **36** (2003) R97.
6. IAEA report, Wienna, Austria 29-30.10.2003, INDC(NDS)-449.
7. J. Tesmer and M. Nastasi (editors), Handbook of Modern Ion Beam Materials Analysis, Materials Research Society (1995).
8. T. Sajavaara, PhD thesis, Report Series in Physics, HU-P-D99, (2002).
9. P.E. Hodgson, The Optical Model of Elastic Scattering, Oxford University Press, (1963).
10. L. Veeser and J. Ellis, Nucl. Phys. A **115** (1968) 185.
11. A.M. Lane and R.G. Thomas, Rev. Mod. Phys. **30** (1958) 257.
12. A. R. Barnett, D. H. Feng, J. M. Steed, L. J. Goldfarb, Computer Physics Communications **8** (197) 4377.
13. H.H. Andersen, F. Besenbacher, P. Loftager and W. Möller Phys. Rev. A **21** (1980) 1891.
14. J. F. Ziegler, J. P, Biersack, U. Littmark, ”The Stopping and Range of Ions in Solids,” vol. 1 of series ”Stopping and Ranges of Ions in Matter,” Pergamon Press, New York (1984).
15. M. E. Brandan and G. E. Satchler, Phys. Rep. **285** (1997) 143.
16. SIGMABASE website: http://www.mfa.kfki.hu/sigmabase/ or http://www.physics.isu.edu/sigmabase/
17. A. Gurbich, SIGMACALC software, private communication.
18. M. Mayer, J. Roth and K. Ertl, Nucl. Instr. and Meth. B **190** (2002) 405.
19. H. S. Sherif, Phys. Rev. C **19** (1979) 1649.
20. D.C. Dodder, G. M Hale, N. Jarmie, J. H. Jett, P. W. Keaton, Jr , R. A. Nisley and K. White, Phys. Rev. C **15**, 2 (1977) 518.
21. A. Gurbich, Nucl. Instr. and Meth. B **131-138** (1998) 60.
22. M. L. West, C. M. Jones, J. K. Bais and H. B. Willard, Phys Rev. **179** (1969) 1047.
23. A. Gurbich, Nucl. Instr. and Meth. B **129** (1997) 311.

24. R. O. Nelson, E. G. Bilbuch, C. R. Westerfeldt and G. E. Mitchell, Phys. Rev. C **29** (1984) 1656.
25. A. Gurbich, Nucl. Instr. and Meth. B **145** (1998) 578.
26. J. W. Olness, W. Haeberli and H. W. Lewis, Phys. Rev. **112** (1958) 1702.
27. F. G. Perey, Phys. Rev. **131** (1963) 745.
28. F. D. Becchetti and W. Greenless, Phys. Rev. **182** (1969) 1190.
29. P. Tischhauser, R. E. Azuma, L. Buchmann, R. Detwiler, U. Giesen, J. Görres, M. Heil, J. Hinnefeld, F. Käppeler, J. J. Kolata, H. Schatz, A. Shotter, E. Stech, S. Vouzoukas, and M. Wiesher, Phys. Rev. Lett **188** (2002) 072501-1.
30. A. Gurbich, Nucl. Instr. and Meth. B **161-163** (2000) 125.
31. B. K. Barnes, T. A. Belote and J. R. Risser, Phys. Rev. **140**, 3B (1965) 616.
32. Hao-Shen, Huanchen-Cheng, Jiajong-Tang and Fujia-Jang, Nucl. Instr. and Meth. B **90** (1994) 593.
33. Å. Bredbacka, M. Brenner, K.-M. Källman, P. Manngård, Z. Máté, S. Szilágyi, L. Zolnai, Nucl. Phys A **574** (1994) 397.
34. J. E. Poling, E. Norbeck and R. R. Carlson Phys. Rev. C **5** (1972) 1819.
35. J. Saarilahti and E. Rauhala, Nucl. Instr. and Meth. B **64** (1992) 734.
36. M. Luomajärvi, E. Rauhala and M. Hautala, Nucl. Instr. and Meth. B **9** (1985) 255.
37. D. C. Ingram, A. W. McCormick, P. P. Pronko, J. D. Carlson and J. A. Woollam, Nucl. Instr. and Meth. B **6** (1985) 430.
38. D. G. Ivey, D. Wang, R. Bruce and D. Knight, J. Electron. Mater **23** (1995) 441.
39. F. Pástzi, Nucl. Instr. and Meth. B **66** (1992) 83.
40. P. Goppelt, J. Biersack, B. Gebauer, D. Fink, W. Bohne, M. Wilpert and T. Wilpert, Nucl. Instr and Meth. B **80-81** (1993) 142.
41. P. Goppelt, B. Gebauer, D. Fink, M. Wilpert, T. Wilpert and W. Bohne, Nucl. Instr and Meth. B **68** (1992) 235.
42. W. Assmann, J. Davies, G.Dollinger, J. Forster, H. Huber, T. Reichelt and R. Siegele, Nucl. Instr and Meth. B **118** (1996) 242.
43. M. Bozoian, K. Hubbard and M. Nastasi, Nucl. Instr. and Meth. B **51** (1990) 311.
44. M. Bozoian, Nucl. Instr. and Meth. B **56/57** (1991) 740.
45. J. Tang, Y. Sun H. Cheng and H. Shen, Nucl. Instr. and Meth. B **74** (1993) 491.
46. A. Nurmela, PhD thesis, Report Series in Physics, HU-P-D89, (2001).

47. S. Nagata, S. Yamaguchi, Y. Fujino, Y. Hori, N. Sugiyama and K. Kamada, Nucl. Instr. and Meth. B **6** (1985) 533.

48. E. Rauhala, J. Appl. Phys. **56** (1984) 3324.

49. P. Bauer, E. Steinbauer and J. P. Biersack, Nucl. Instr. and Meth. B **79** (1993) 443.

50. K. Arstila, T. Sajavaara and J. Keinonen, Nucl. Instr. and Meth. B **174** (2001) 163.

51. T. Sajavaara, K. Arstila, A. Laakso and J. Keinonen, Nucl. Instr. and Meth. B **161-163** (2000) 235.

52. I. M. Sobol, ”The Monte Carlo Method”, Mir Publishers, Moscow (1975).

53. M. Tosaki, S. Ito and N. Maeda, Nucl. Instr. and Meth. B **168** (2000) 543.

54. A. F. Gurbich, N. P. Barradas, C. Jeynes and E. Wendler, Nucl. Instr. and Meth. B **190** (2002) 237.